# Failure Modes of Insulating Pressboard Subjected to High Electric Fields and Durations: Evidence of Partial Discharge and Changes at the Microscopic Scale

Yongqiang Wang,* Ruoyu Fei, Changhui Feng, and Sen Fang

The deterioration of insulation pressboard under needle-plate discharge was tested, and the degradation stage was divided according to observed experimental phenomena. Based on the improved Top-hat watershed image segmentation method, the white marks area of the pressboard were tested. Fibres with different discharge states were extracted from SEM images. The fibre width was calculated, and the porosity of the surface of the insulation pressboard at different degradation stages was calculated. Simultaneously, the 3D reconstruction technique was used to observe the 3D morphology of fibres at different discharge stages. The study found that with the deepening of the discharge process, the discharge of the pressboard increased, and the white marks of the pressboard continued to expand from point to surface. In addition, the diameter of the fibre of the insulating pressboard decreased obviously with the increase of the pressing time, and the fibre diameter was 89.6% after the breakdown. Moreover, the electrical stress had a great effect on the expansion of the interlayer pores of the pressboard; the cross-section porosity of the insulating pressboard gradually increased with the deepening of the discharge process, and after breakdown, the interlayer porosity reached 12.5%.

*Keywords: Insulation pressboard; Image processing; Fibre; Scanning electron microscope*

*Contact information: Hebei Provincial Key Laboratory of Power Transmission Equipment Security, Department of Electrical Engineering, North China Electric Power University, Baoding 071003, China; *Corresponding author: qianghd@126.com*

## INTRODUCTION

The power transformer is an important part of transmission and distribution equipment for power systems, and partial discharge is one of the causes of insulation damage in electrical equipment (Tatsuki *et al.* 2017). However, in the process of transformer production, transportation, and operation, insulation materials often suffer latent defects and gradually deteriorate. Eventually, these defects will cause damage to the equipment (Khawaja and Blackburn 2009). Therefore, it is meaningful to improve the insulation performance of a transformer and study the discharge characteristics and microscopic characteristics of oil-paper insulation.

Many scholars have investigated partial discharge. For example, Mitchinson *et al*. (2008) designed a slanted tip oil-paper insulation creeping discharge model, which shows that the main causes of flashover of the oil-paper insulation and final flashover accidents are the high duration and high field strength for a sufficient duration. Zainuddin *et al.* (2013) and Yi *et al.* (2011) found that, with the development of partial discharge, white creep marks would appear on the surface of the insulating paperboard. The white mark

indicates the discharge development; it is an external manifestation of the internal gas channels. A large number of tiny bubbles can be extracted from the white spot area. As the bubbles generated during the development of partial discharge change the light scattering coefficient of the cardboard, these areas become white marks. As the white marks continues to expand, an arc eventually appears and flashes through along the white mark path. Finally, the intense partial discharge energy causes carbonization of the insulating cardboard fibres, which turns white spots into black carbon marks. Thus, these creep marks can reflect the development of surface discharge to some extent. In another study, Yan *et al.* (2012) studied the bulk properties of the impregnated insulating paper, and the dielectric constant and electrical conductivity of insulating paper during damage thereto were analysed.

In addition, with the development of science and technology, researchers began to study the microscopic characteristics of insulation materials, *via* scanning electron microscopy (SEM). Some researchers used MATLAB™ to detect fibre edges in SEM images and calculated the hole size and fibre roughness (Wang *et al.* 2018). Other studies found that cellulose was destroyed by the decomposition of lignin and hemicellulose (Verma *et al*. 2004), and the change in oil-paper surface microstructure in the accelerated thermal aging process was evaluated (Wei *et al.* 2015). Others divided the development stage of partial discharge in oil-pressboard insulation with needle-plate electrodes according to the characteristic parameters of different periods (Li *et al.* 2017). However, most findings were obtained only by observing the pictures with the naked eye, and the pictures were not analysed in depth.

Image processing has gradually developed in recent years and is used in medicine and industry (Dong *et al.* 2018; Jia *et al.* 2018; Niu *et al.* 2018; Sun *et al.* 2018). In the study of PD, researchers have rarely studied the deterioration of insulating paperboard at each stage of the discharge, and the discharge phenomena and statistics of cardboard microdata need to be further improved.

In this paper, after pre-processing of SEM images (*e.g.*, by noise reduction and filtering), image segmentation is applied to extract the part that needs to be observed, and the changes in microscopic characteristics in the process of partial discharge of insulating oil-paper can be observed more clearly. According to the phenomena seen in the discharge process, the partial discharge process of insulation pressboard is divided into four stages. At the same time, based on computer technology, the microscopic characteristics of pressboard in different discharge stages were studied by the following means: image processing; the 3-D model of pressboard fibre was constructed by 3-D reconstruction method; microscopic information was obtained, measuring the white spot area, fibre width and porosity of the paperboard at each stage. The dimensional information was calculated, thereby establishing the development law of each feature, and this was used to characterize the degree of pressboard deterioration under partial discharge.

This paper proposes a new idea for observing the insulation performance of cardboard. It conducts external macro observation and measurement of oil-impregnated paper insulation partial discharge and detects and counts the internal micro-information after insulation paper discharge. Through the combination of these two aspects, it is convenient to further study the mechanism of partial discharge in oil-paper laminated insulation.

## EXPERIMENTAL

### Design of Discharge Experiment of Insulation Pressboard

Standard insulation pressboard, 80 × 80 × 2 mm, and Karamay 25# transformer oil were used for this experiment. The insulating pressboard was made from ultra-high voltage transformer pressboard and it is mainly made of wood pulp, which is mainly composed of cellulose, hemicellulose, and lignin. The density of the insulation paper used in this paper is 1.20 g/cm$^3$, the relative dielectric constant (before the experiment) is 3.59, and the insulation resistivity is $6.25\times10^{13}$ Ω·m. Before the discharge experiment, these materials were placed in a vacuum oven at a temperature of 90 °C and a pressure of 50 Pa for 24 h to remove moisture and gases present. Subsequently, the temperature was adjusted to 80 °C, and the pressboard was immersed in the transformer oil and vacuum-impregnated for 12 h. (Cui *et al.* 2017; Wang *et al.* 2019)

The partial discharge device used a vertical creeping discharge structure. It consisted of a needle electrode with a length of 30 mm, a diameter of 1 mm, a tip curvature of 30°, a brass plate with a diameter of 100 mm, and a thickness of 20 mm. The whole experimental platform is shown in Fig. 2 (Wang *et al.* 2019, 2020). It comprised a booster console, experimental transformer, protective resistor, coupling capacitor, and smooth aluminium conductor. At the same time, the discharge process was recorded using a camera.

The discharge experiment was conducted using the constant pressure method. When testing with high voltages, pressure measurement was carried out at a step rate of 1 kV/s. When the discharge signal of the partial discharge tester was stable, the voltage was held constant for 5 min and this voltage value was denoted as the initial discharge voltage $U_0$, where $U = 1.2U_0$, and then $U$ was applied as a constant voltage on the pressboard until the it broke down. The results of measurement of the initial discharge voltage of five samples are as listed in Table 1. The average initial discharge voltage of the five samples was 14.3 kV. Therefore, the constant voltage test was carried out at about 1.2 $U_0$, or about 17.2 kV.

**Table 1.** Initial Discharge Voltage Statistics of PD

| Test sequence | 1 | 2 | 3 | 4 | 5 | Average |
|---|---|---|---|---|---|---|
| Initial discharge voltage/ kV | 14.3 | 14.7 | 14.2 | 13.8 | 14.5 | 14.3 |

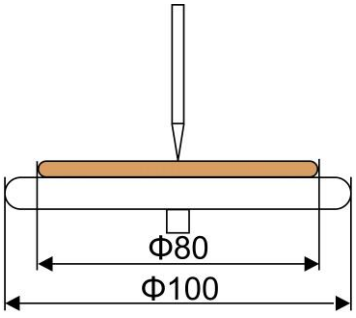


**Fig. 1.** Needle plate discharge device

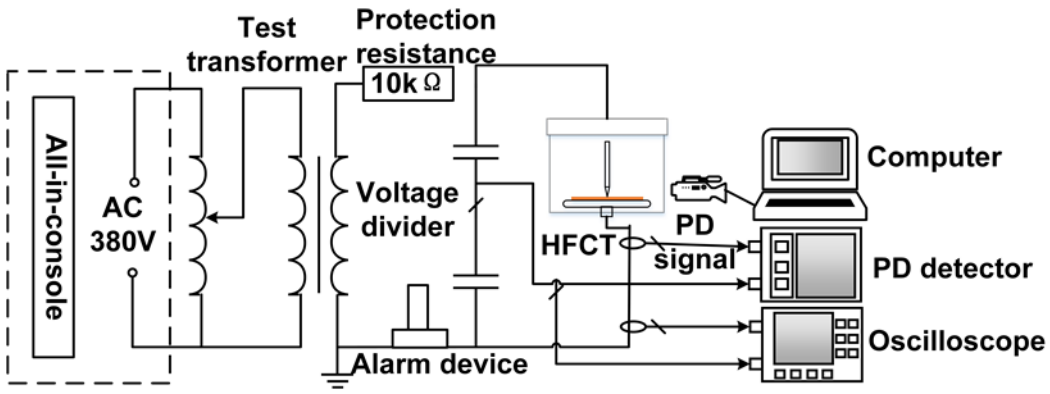


**Fig. 2.** Discharge experimental platform

## Image Segmentation with Watershed Algorithm

The main purpose of extracting fibre profiles from SEM images is to find segmentation points of fibre profiles and their background. Due to their similar colour, common segmentation methods cause over-segmentation; thus, the watershed image segmentation algorithm was selected based on a top-hat transformation in this research.

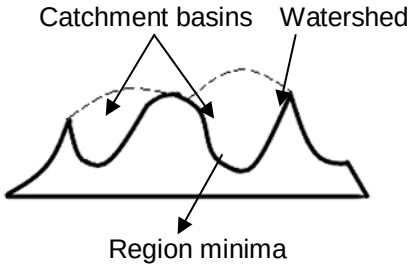


**Fig. 3.** Schematic diagram of the watershed segmentation algorithm

The watershed segmentation algorithm is shown in Fig. 3. The aim is to treat each SEM image as a topological geomorphology map. Each pixel grey value is the elevation of that point; the local minimum in an area represents the catchment basin; and the surrounding boundary represents the watershed. It is assumed that a small hole is punctured in the catchment basin, and water is injected continuously from the hole. With increasing depth, the area of influence of each local minimum gradually expands outward, forming a watershed at the junction of the two collection basins (Vincent and Soille 1991). The gradient function is as follows,

$$G(x,y) = grad\big(f(x,y)\big) = \{[f(x,y) - f(x-1,y)]^2 + [f(x,y) - f(x,y-1)]^2\}^{\frac{1}{2}} \quad (1)$$

where $f(x,y)$ represents the original grey-scale image, and $grad(\bullet)$ represents the gradient operation, since the individual watershed segmentation algorithm is prone to over-segmentation when extracting an unknown subject line. Although the boundary between fibre and background is more obvious, the fibres are of similar colour; therefore, it is necessary to split the image twice. In the first segmentation process, the OTSU algorithm can be used to segment the fibres from the background. The second time, a top-hot based watershed segmentation algorithm is applied to segment the fibres.

The OTSU (Du *et al.* 2019) is an algorithm for obtaining a binary image with which to segment the threshold. The main principle is to use the characteristics of the grey image

to divide the picture into two parts: background and foreground. Setting the segmentation threshold of fibre and background as "$T$", in the binarised image, the ratio of the number of pixels of the fibre "$N_0$" to the entire image is $\omega_0$, the average grey-scale is "$\mu$"$_0$, the ratio of the number of pixels "$N_1$" in the background to the total number of pixels is "$\omega_1$", the background average grey-scale is "$\mu_1$", the average grey level of the image is "$\mu$", and the class square error is recorded as "$g$", the pixel points of the image length and width are "$M$" and "$N$" respectively, then:

$$\begin{cases} \omega_0 = N_0/(MN) \\ \omega_1 = N_1/(MN) \end{cases} \tag{2}$$

$$\begin{cases} N_0 + N_1 = MN \\ \omega_0 + \omega_1 = 1 \\ \mu = \omega_0\mu_0 + \omega_1\mu_1 \\ g = \omega_0(\mu_0 - \mu)^2 + \omega_1(\mu_1 - \mu)^2 \end{cases} \tag{3}$$

If the $g$ is maximised, the threshold $T$ is the required value, and the first divided image $f'(x, y)$ is obtained.

Then, the watershed segmentation algorithm is used for the second step:

$$G(x, y) = grad\big(f'(x, y)\big) \tag{4}$$

Finally, the top-hat opening operation is used to operate the watershed image, selecting the appropriate structure $b$ to operate on $G$, $G \ominus b$ for erosion operation, $G \oplus b$ for dilation operation,

$$G' = G \circ \mathrm{b} = G \ominus b \oplus b \tag{5}$$

where $b$ is composed of three basic structural elements:

$$b_1 = \begin{bmatrix} 0 & 0 & 0 \\ 1 & 1 & 1 \\ 0 & 0 & 0 \end{bmatrix} \quad b_2 = \begin{bmatrix} 0 & 1 & 0 \\ 0 & 1 & 0 \\ 0 & 1 & 0 \end{bmatrix} \quad b_3 = \begin{bmatrix} 0 & 1 & 0 \\ 1 & 0 & 1 \\ 0 & 1 & 0 \end{bmatrix} \tag{6}$$

Substituting $b_1$, $b_2$, and $b_3$ into Equation 5 to obtain $G'_1$, $G'_2$, and $G'_3$, and assigning different weights $\alpha_1$, $\alpha_2$, and $\alpha_3$ to obtain $G'$, which is the final fibre extraction image:

$$G' = \alpha_1 G'_1 + \alpha_2 G'_2 + \alpha_3 G'_3 \tag{7}$$

The segmentation results of original SEM images (Fig. 4a) using the above segmentation algorithm are shown in Fig. 4b.

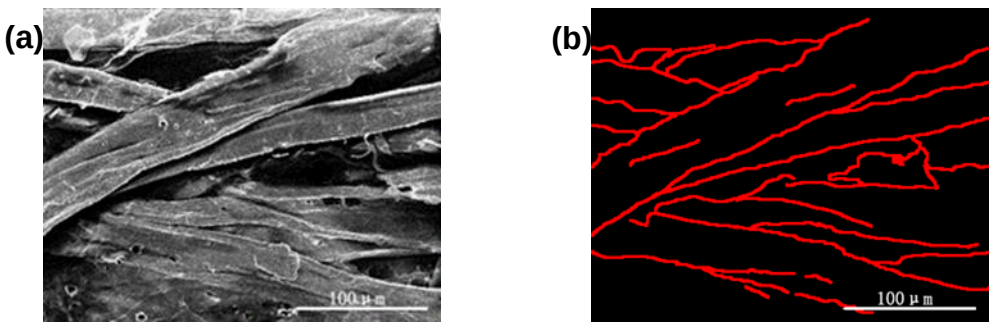


**Fig. 4.** SEM micrograph of insulation pressboard: (a) The original image ×500, (b) Results of fibre contour image segmentation (marked resolution:397×314 Pixels)

## Measurement Parameters

*White marks area*

To study the discharge characteristics of the surface discharge of the insulation pressboard under the needle plate model, the surface discharge white marks area of the insulating pressboard was selected as one of the discharge development criteria. The extent to which the tip discharge is destructive to the surface of the insulation pressboard could be determined by considering the white marks area. According to the image processing method used here, after adjusting the pressboard photos uniformly to 256 × 256 pixels, the white marks area was determined from images of the pressboard and the proportional area of the white marks was calculated.

In image processing, each picture is composed of pixels. Firstly, the RGB image was pre-processed to increase the colour contrast of the white marks and the pressboard, so that the white mark edge was more obvious. Secondly, it was converted into a grey-scale image. The colour distribution of the pixels in the grey-scale image is 0 to 255. When the grey value is 0, the pixel appears black, and when the grey value is 255, it appears white. After using image processing to improve the contrast, the white marks in the grey-scale image contrasted with the surrounding pressboard. Using MATLAB™ software, and setting a threshold T, the grey-scale image was further converted into a black and white image. Finally, using an editing program to calculate the total number of pixels and the number of white pixels in the picture, which were denoted as S and s respectively we calculated the ratio of the number of white marks pixels in the whole picture at each stage:

$$\boldsymbol{ratio} = \frac{\boldsymbol{s}}{\boldsymbol{S}} \times \mathbf{100}\% \quad (8)$$

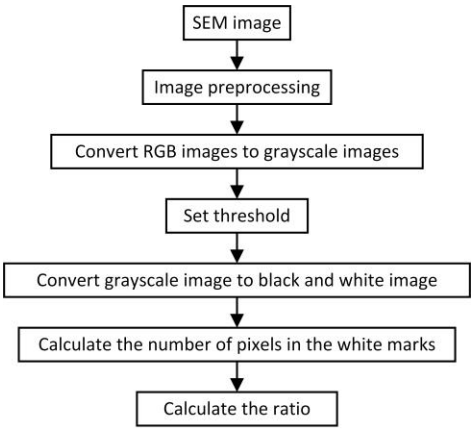


**Fig. 5.** White marks area calculation flow chart

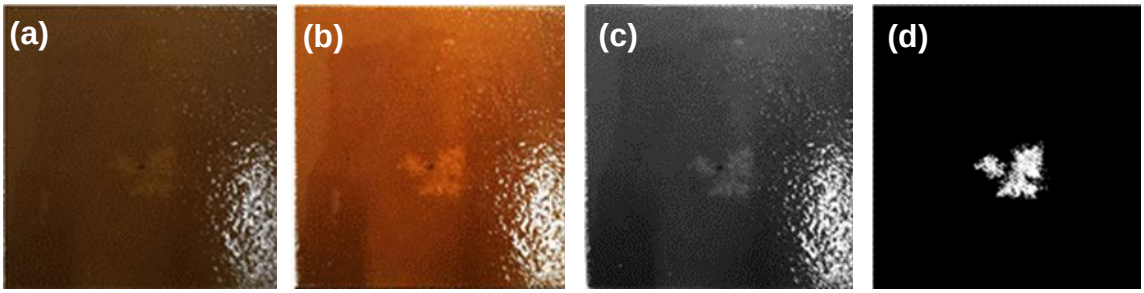


**Fig. 6.** Insulating pressboard white mark extraction: (a) The original image, (b) Improve contrast, (c) Grayscale image, (d) Black and white graph

*Fibre width*

Most researchers use the MATLAB™ tool-kit to measure the diameter, but this method is inaccurate. The pressboard fibre tends to be curved and the thickness is unevenly distributed. Therefore, it is necessary to find the correct direction of the fibre, use this as the axis to measure the width in multiple places, and obtain the average value. The measurement flow chart is as shown in Fig. 7. To detect the fibre width, the aforementioned watershed segmentation algorithm based on a top-hat function is used to segment the image and extract the fibre contour (*e.g.*, Fig. 8).

The specific steps for measuring the width using the central axis method are as follows: the first step is to determine the direction and choose a point next to the outline, denoted as $A$. Second, take $A$ as the starting point, plot straight lines along the $X$ and $Y$ −directions, and observe the intersection of the two straight lines and the fibre outline. If the distance between the two intersections in the $X$ −direction is greater than that in the $Y$ −direction, the fibre is measured in the $Y$-direction and *vice versa*. As shown in Fig. 9a, it is seen that the fibre should be measured in the $Y$ −direction.

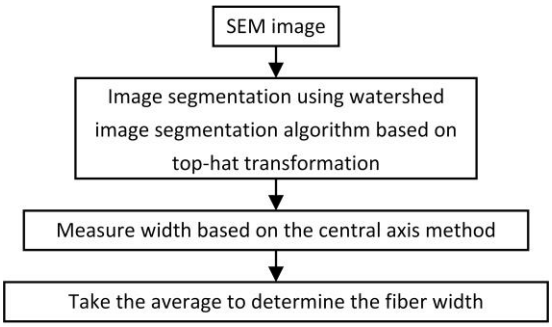


**Fig. 7.** The flow chart of fibre width measurement

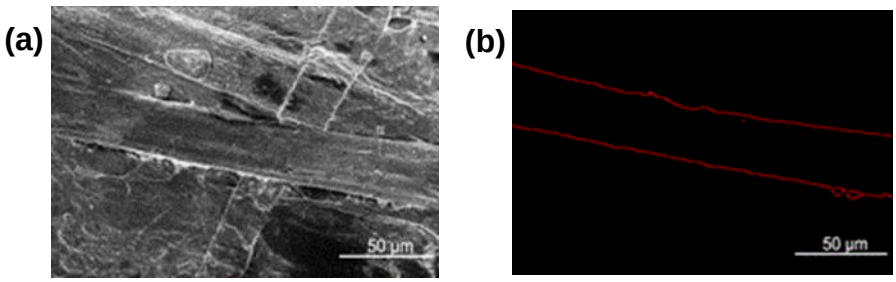


**Fig. 8.** SEM micrograph of insulation pressboard: (a) insulating pressboard SEM original image×1000, (b) insulating pressboard fibre edge extraction map

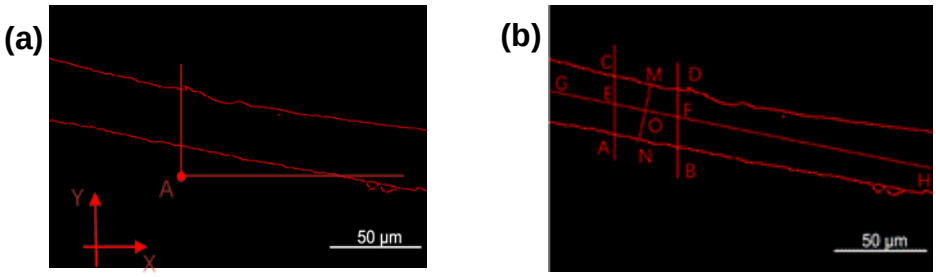


**Fig. 9.** Central axis method for measuring fibre width: (a) Determine direction, (b) Measure width

Two points $A$ and $B$ were chosen. These were close to each other on the fibre, and a straight line was plotted in the $Y$-direction, intersecting the fibre at $C, D$. The points $AC$ and $BD$ were connected. Their mid-points $E, F$ respectively were found and connected $EF$. Finally, the mid-point $O$ of $EF$ was determined. Then $O$ was passed as the vertical line of $EF$, and the fiber contour was crossed to $M,\ N$. It was assumed that $MN = l$, that is, the width of a fibre. These steps were repeated many times, calculating $l$, and taking the average value thereof.

*Porosity*

When using SEM images to observe the fibres, researchers seldom have observed the internal cross-section of the insulation pressboard. Here, the cross-sectional pore profile was extracted by the above segmentation algorithm and the porosity in different discharge states was analysed.

Figure 11a shows the cross-sectional image of the insulating pressboard, and the pores appear black on the image, which provides a contrast with the colour of the fibre. According to this feature, the porosity of the material can be calculated where $\xi$ is the porosity, $s_b$ is the pore area (the number of black pixels), and $S$ is the product of the cross-sectional area:

$$\xi = \frac{s_b}{S} \tag{9}$$

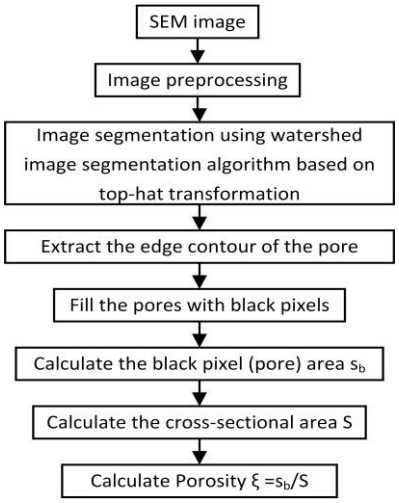


**Fig. 10.** Porosity calculation flow chart

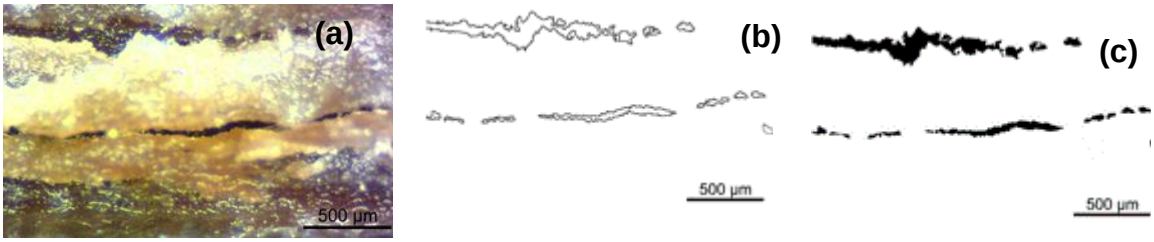


**Fig. 11.** Insulating pressboard cross-section pore extraction diagram: (a) Cross-section of insulating pressboard, (b) Extract the edge of the insulating pressboard cross section, (c) Filled insulation pressboard cross section pore

The process involves adjusting the contrast and colour saturation of the image, pre-processing it to make the pore-fibre boundary clearer. Then the top-hat based watershed segmentation algorithm was used to segment the image to extract the pore boundary. Subsequently, the pores were filled with black pixels, thus obtaining the pore area "$s_b$ " (that is, the number of black pixels) and the cross-sectional area " $S$ ", so as to obtain the porosity.

## 3D RECONSTRUCTION OF INSULATION PRESSBOARD FIBRE

The 3-D reconstruction of material microstructure combines image processing and computer technologies. The 2-D information about the material can be obtained by computer, and then the 3-D spatial model of material can be reconstructed.

As the SEM pictures can only show the surface of the insulation pressboard fibre morphology, the inner layer of the pressboard cannot be observed. To observe the internal microscopic morphology of the insulating pressboard, the complete sequence cross-section image of the sample was obtained by polishing the cross-section of the pressboard and reconstructing the associated 3-D model.

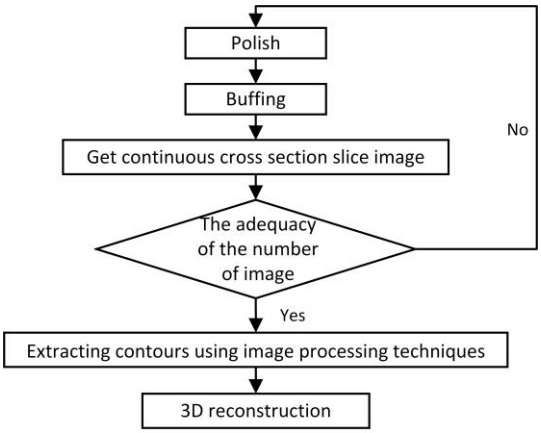


**Fig. 12.** Flowchart for 3-D reconstruction of insulation pressboard fibre

The process was as follows:

1) Cut the pressboard into 2 mm × 10 mm × 10 mm cuboids (length × width × thickness).

2) Place the sample under an optical microscope and use a point on the edge as a fixed observation point.

3) 5000 mesh emery paper is used to polish the pressboard along the cross-section. After each polishing stage, measure the thickness of the sample block with a micrometre, and control the thickness of the polish to about $10 \pm 2$ μm.

4) Buff the sample block, and obtain the cross-sectional images of this fibre bundle layer under the microscope (Miao *et al.* 2017).

5) Repeat Steps 2 to 4 to obtain 100 consecutive cross-sectional slice images.

6) Pre-process the original image, by, for example: contrast expansion, image noise reduction, *etc*.

7) Extract the contour of the fibre to be extracted using the aforementioned segmentation algorithm.

8) Repeat Steps 6-7 to extract the desired fibre profile from 100 cross-sectional images.

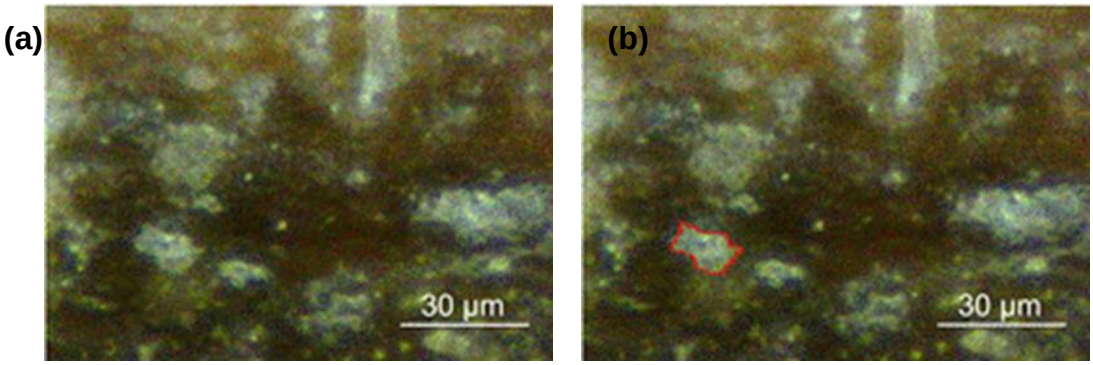


**Fig. 13.** Insulated pressboard cross section image: (a) Insulated pressboard cross section image, (b) Pressboard cross-section fibre profile extraction

9) Pre-process the contours. Due to problems such as placement of the sample under the microscope and the accurate focussing thereof, the centre position of the adjacent two cross-section fibre outlines may vary greatly. Therefore, it is necessary to make the centre points of adjacent contour lines coincide so that the size ratio is the same (Eqs. 9 and 10) (Ma *et al.* 2007). The specific approach is to assume that the fibre profiles of adjacent cross sections are $Contour_1$, $Contour_2$. The coordinates of the center point are $center_1(x_1, y_1)$, $center_2(x_2, y_2)$, width and height are $(width_1, height_1)$, $(width_2, height_2)$, the translation distance and scaling factor of the profile are $PanFactor$ and $ZoomFactor$, respectively. Then, the coordinates of each point on the $Contour_1$ are kept unchanged, and the $Contour_2$ coordinates are adjusted using the following equation.

$$\begin{cases} PanFactor_{.x} = x_2 - x_1 \\ PanFactor_{.y} = y_2 - y_1 \\ ZoomFactor_{.x} = width_2/width_1 \\ ZoomFactor_{.y} = height_2/height_1 \end{cases} \tag{9}$$

$$\begin{cases} Contour_{2.x} = (Contour_{1.x} + PanFactor_{.x}) \times ZoomFacto_{.x} \\ Contour_{2.y} = \left(Contour_{1.y} + PanFactor_{.y}\right) \times ZoomFactor_{y} \end{cases} \tag{10}$$

10) Construct a triangular mesh model using the shortest diagonal method. Assume that the pixel points of the fibre profiles in two adjacent cross-sections are, respectively, $P_i$, $Q_i$, and call $P_iP_{i+1}$ and $Q_iQ_{i+1}$ the line segment of the contour. If the two endpoints of a contour line segment are connected to a point on the contour line of the adjacent cross section, it forms a triangular face. The so-called 3-D reconstruction with contour is to connect the contour lines of two surfaces with a series of triangular faces. Since the contour has been pre-processed, the shortest diagonal method can be used to construct the triangular mesh model, the shortest distance between two adjacent contour points can be calculated by the following equation:

$$D = \sqrt{(P_x - Q_x)^2 + \left(P_y - Q_y\right)^2} \tag{11}$$

where $(P_x, Q_x)$ are the coordinates of the current point, and $(P_y, Q_y)$ are the coordinates closest to the current point. In this method, all contour lines are connected to form a triangular mesh model.

11) Render the triangular mesh model and complete the reconstruction.

Figure 14 shows the 3-D model of the fibres. The construction of the 3-D model of a fibre overcomes the limitation of a 2-D image where only surface fibres can be observed. Using 3-D reconstruction techniques, fibres can be more clearly observed from different angles to see the contours of the fibre, the surface roughness, internal holes, and staggered distributions thereof.

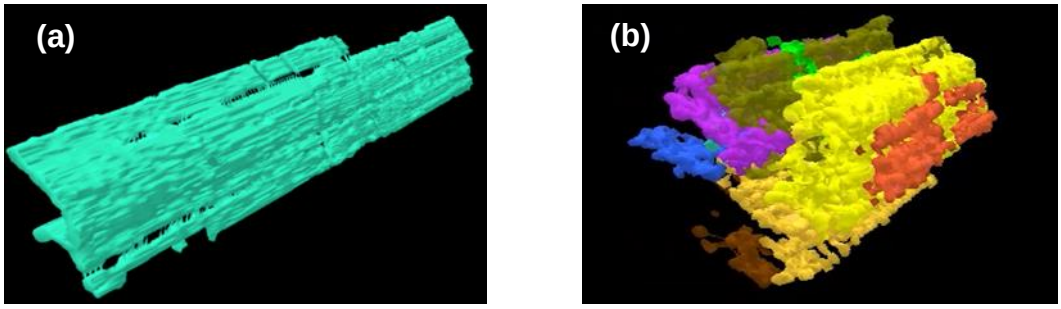


**Fig. 14.** 3-D model of fibres: (a) 3-D model of a single fibre, (b) 3-D model of a fibre group

## RESULTS AND DISCUSSION

### White Marks Area and PD Quantity of Pressboard in Different Stages

The discharge experiment was conducted using the constant pressure method. After re-observation of the experimental video footage, according to the phenomenon difference in the development of oil-paper insulation discharge at different ages, the development process of the needle-plate discharge of the insulation pressboard can be divided into four stages: an initial stage, a discharge development stage, a discharge burst stage, and a breakdown stage. At the initial stage, there was no obvious spark, and a large number of small diameter bubbles were precipitated at the junction between the needle electrode and the insulation pressboard, which formed a conical shape and diffused upwards. Over time, at the point of the tip, a light white mark appeared. During the discharge development stage, the bubbles gradually diffused around the pressboard, and the overflow site was not limited to the vicinity of the tip, the bubbles grew in diameter but decreased in number, carbon trace began to form on the insulation pressboard, and the colour of the white mark deepened. During the discharge burst stage, the area of the white marks increased, the discharge was audible, and the bubble underwent precipitation over a larger area; when the insulation pressboard broke down, it was accompanied by a spark and the generation of smoke. The formation of the white mark was mainly attributed to the intense PD concentrated in the region of the tip. A large amount of energy was generated during the discharge process, which forced the insulation oil and water to overflow from the surface of the pressboard. Some of the water gradually broke down into bubbles, but it could not diffuse freely due to the influence of the surrounding liquid. Simultaneously, the reflection index of the pressboard is affected by these bubbles, thus forming white marks. After conducting multiple sets of experiments, the time period of each stage of statistics is shown in Table 2.

Because the insulation pressboard is difficult to recover once it is damaged during the pressure test, it is not feasible to withdraw the insulation paper and return to the test platform after a period of withstand voltage testing. To solve this problem, the withstand voltage test was carried out in stages but the withstand voltage time was increased each

time. That is, the pressboard with withstand voltages of 1 h, 7 h, and 13 h and the pressboard after breakdown were respectively taken as samples of "initial discharge", "discharge development period", "discharge outbreak period" and "breakdown". Using image processing techniques to calculate the white marks area on each sample (Table 3). At the same time, the PD (partial discharge) quantity was recorded every 1 h (Fig. 16).

**Table 2.** Appearance Period of Each Stage

| Stage | Initial stage | Discharge development stage | Discharge burst stage | Breakdown stage |
|---|---|---|---|---|
| Time | 0~2h | 2h~12h | 12h~14h | 14h15min |

**Table 3.** White Mark Area of PD at Each Stage

| Stage | Initial stage | Discharge development stage | Discharge burst stage | Breakdown stage |
|---|---|---|---|---|
| white marks area (pixel) | 311 | 1502 | 6074 | 6698 |
| Ratio | 0.47% | 2.29% | 9.27% | 10.22% |

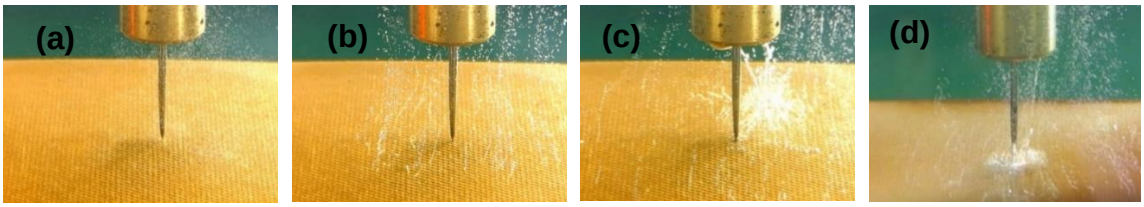


**Fig. 15.** Insulation pressboard needle-plate PD development
(a) Initial stage (b) Discharge development stage (c) Discharge burst stage, (d) Breakdown stage

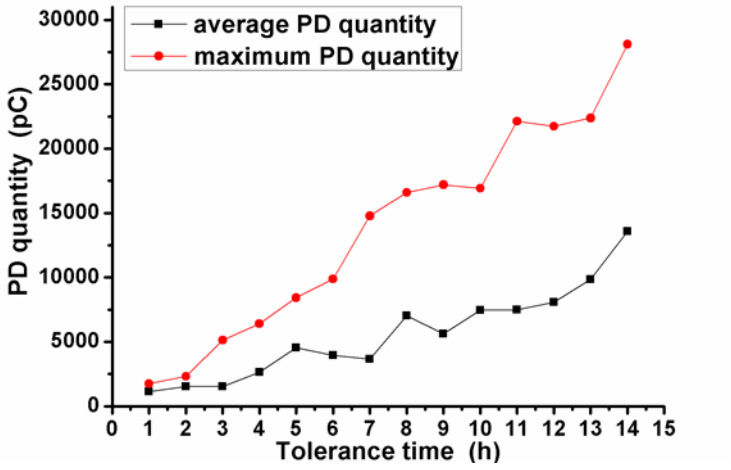


**Fig. 16.** Variation of discharge quantity in the PD process

During the experiment, it was found that as the pressing time was increasing, the white spot gradually expanded outward from the point to the surface with the needle tip as the centre, and the white marks diffusion area overlapped with the bubble generation area. The bubble precipitation area continued to increase as the white marks area expanded. In the initial stage of the discharge, the white spot spread slowly and had a small area. After the discharge development period, the white marks spread rapidly. When the discharge

burst period was reached, the white marks area accounted for 9.27% of the total area of the pressboard, which was 19.7 times the initial discharge. The white spot area reached 10.22% during breakdown. Combined with the discharge volume, it is found that the PD quantity of the pin-plate discharge generally showed an upward trend. Simultaneously, the development law is similar to the white mark diffusion law. At the initial stage (1 to 2 h), the PD quantity was small and stable. To the development period (2 to 12 h), the PD quantity increased obviously, although it occasionally decreased, but the overall upward trend, and the rate of increase had increased obviously from the initial stage. After entering the discharge burst period, the PD quantity further increased at a faster rate until breakdown. Therefore, it is speculated that the expansion process of white mark on pressboard is closely related to the change process of partial discharge, and the area of white marks can be used as one of the discharge development criteria.

## Microscopic Characteristics of Pressboard and Analysis Thereof

SEM was used to observe the surface morphology of the insulating pressboard at different discharge periods (Fig. 17).

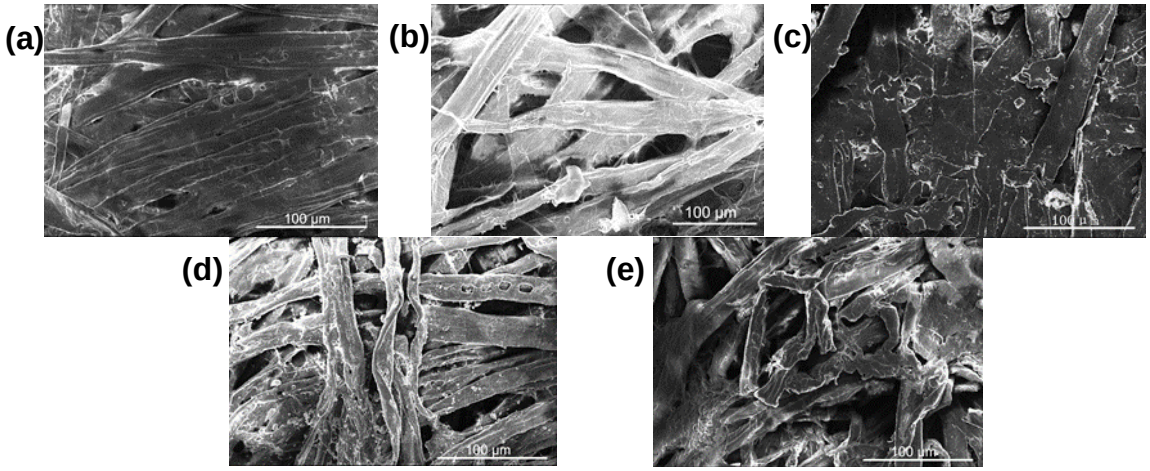


**Fig. 17.** SEM micrographs of insulation pressboard at different discharge stages
**(a)** SEM image of untreated insulation pressboard×500,
**(b)** SEM image of insulation pressboard at the initial stage×500,
**(c)** SEM image of insulation pressboard at the development stage ×500,
**(d)** SEM image of insulation pressboard at the discharge burst stage×500,
**(e)** SEM image of insulation pressboard at the breakdown stage×500,

Using the fibre width measurement and porosity methods described in Section "Measurement Parameters", the variation curves of fibre width and porosity with the deepening of the discharge can be obtained.

Through the SEM image of pressboard (Fig.17) and the curve of fiber width variation (Fig.18), it can be obtained that:

(1) With the increase of pressure time, the surface structure of insulating pressboard was greatly affected by PD effect, and the overall fibre diameter showed a decreasing trend, which could be used as one of the criteria for the development of needle plate discharge.

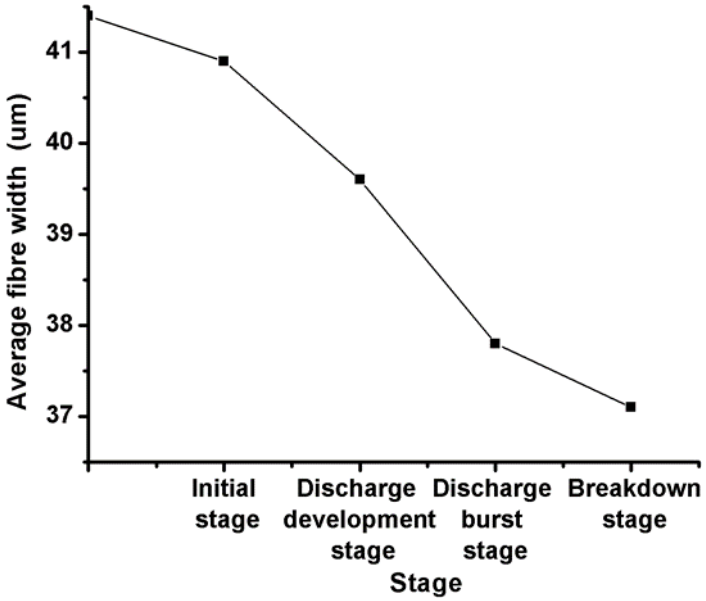


**Fig. 18.** Insulation pressboard fibre width variation in different discharge stages

(2) The fibre width of untreated pressboard was even, arranged closely, and the surface contained a small amount of filament. Compared with untreated pressboard, the surface of the pressboard at the initial stage of discharge was relatively smooth with reduced roughness, and the fibre diameter decreased slightly, but the decreasing trend was only 0.5 μm, indicating that the pressboard at the initial stage of discharge was less affected by partial discharge.

(3) In the development period of the discharge, the fibre diameter of the pressboard was more affected by the discharge compared with the initial stage. The surface loosened, the fibre continuously tore and peeled longitudinally. The fibre diameter decreased faster.

(4) After entering the discharge burst period, the pressboard fibre began to be bent and broken, resulting in polymerization at the fracture, holes, and damages on the surface. Meanwhile, white crystals were produced, and the fibre diameter dropped rapidly until breakdown. After breakdown, the fibre diameter was 89.6% of the untreated pressboard.

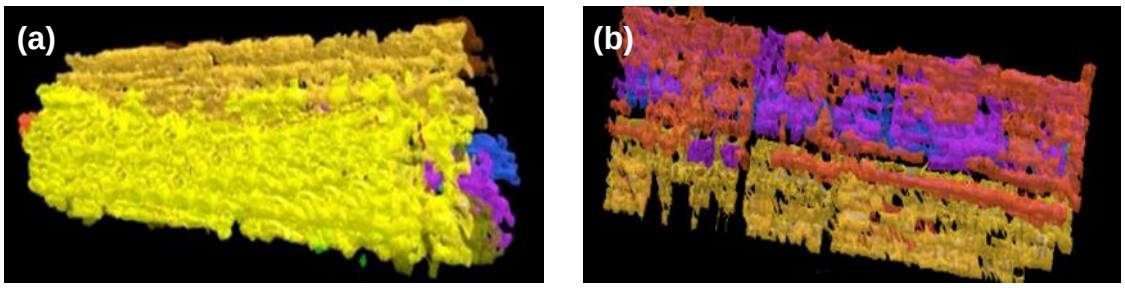


**Fig. 19.** 3-D model of pressboard fibre: (a) 3-D model of pressboard fibre at the initial discharge stage, (b) 3-D model of pressboard fibre at the discharge breakdown stage

Through the 3-D fibre model (Fig. 19) and the porosity change curve (Fig. 20), it can be obtained that:

(1) With the deepening of the PD degree, the pressboard was obviously damaged in the interlayer direction, and the interlayer porosity showed an increasing trend.

(2) The porosity of the pressboard at the initial stage of PD was slightly higher than

that of the untreated pressboard, but it was still relatively flat and the interlayer fibres were compacted.

(3) Upon entering the discharge development stage, pressboard fibres became looser, gradually becoming more sparse, and the rate of pore expansion was accelerated.

(4) Over time, the pore distribution in the cross-section increased, especially in the discharge burst stages. Under the influence of PD, the degradation rate of pressboard accelerated, the interlayer pore crack enlarged, and the porosity reached 11.9%. After the breakdown, the pressboard fibre was seriously damaged, and obvious breakdown marks were found *via* the 3-D model, with the porosity reaching 1.3 times of untreated pressboard fibre.

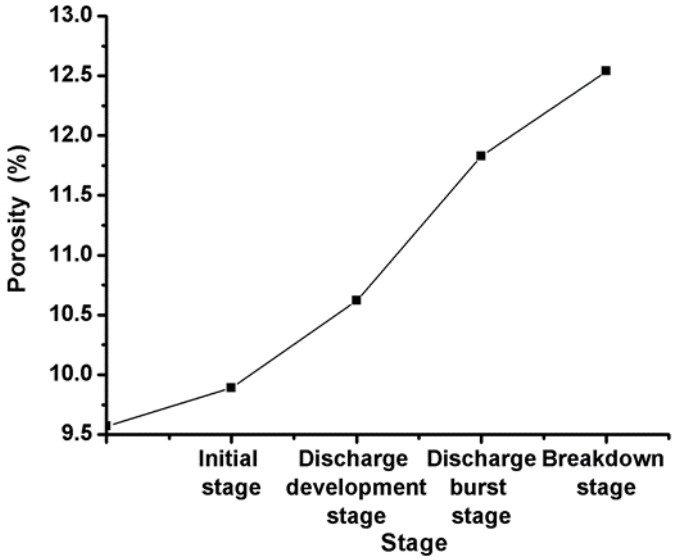


**Fig. 20.** Insulation pressboard porosity variation in different discharge stages

The reason for the above behaviour is that:

(1) The transformer oil was ionised and charged particles were generated under the action of the local high field strength, and the pressboard was continuously subjected to impact movement, damaging the surface of the insulating pressboard (Butcher *et al.* 2006; Kolb *et al*. 2008). The fibre showed the phenomenon of "peeling" and "fusing", resulting in the significant reduction of fibre thickness and length.

(2) Cellulose molecules contain $n\beta$-D-glucopyranose (Fig. 21); however, β-D-glucopyranose is a polyhydric aldehyde, and each β-D-glucopyranose contains three free –OH radicals: -OH belongs to a hydrophilic group, which allows hydrogen bonds to form within each cellulose macromolecule. The fibre binding force is related to the bonding strength of the hydrogen bond. Before the discharge experiment, the cellulose molecules were less damaged, the degree of polymerisation was higher, and the bond energy of the hydrogen bond was also greater. Therefore, the insulating pressboard fibres were more densely packed and the porosity was small. During the discharge process, as the glycosidic bonds broke first, the degree polymerisation of the cellulose began to decrease. The oxygen atom and the hydroxyl group were also gradually broken, which caused the pyran ring to be opened, the cellulose macromolecular chains were broken into small molecular chains, and the intramolecular force was reduced. Meanwhile, the porosity also increased.

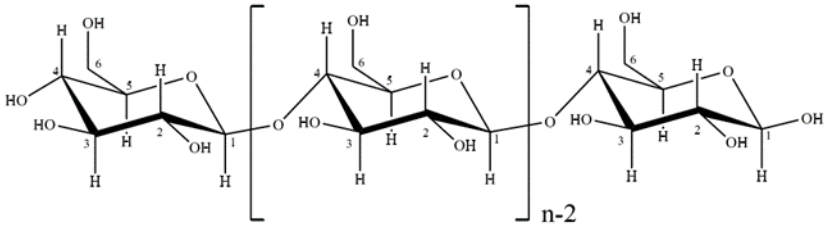


**Fig. 21.** Structure of cellulose molecular chain with degree of polymerisation n

(3) At the initial stage of discharge, the structure of insulating pressboard is tight and there are no bubbles in the pores. The gap between oil-immersed insulating pressboard and transformer oil is relatively small in terms of dielectric constant. Therefore, it is not easy to discharge, the damage to the pressboard is light, and the pore expansion is not obvious. Over time, the discharge generated heat, which decomposed the cellulose in the pressboard and transformer oil, and, as a result, the pores filled with gas. The relative dielectric constant of the gas was low, and the electric field strength was significantly increased, resulting in an uneven distribution of the internal field strength across the insulation pressboard. On the other hand, the discharge was more violent, causing more serious damage to the mechanical properties and electrical insulation properties of cellulose, so that the fibre surface was damaged, the diameter was reduced, and the interlayer porosity was increased.

## CONCLUSIONS

1. Through image segmentation technology, 3-D reconstruction technology can be used in combination to reconstruct the 3D model of the fibre to obtain the surface topography such as fibre splitting and breaking. Also, it is possible to extract the characteristics of the insulating pressboard under different discharge states, analyze and obtain the development of white marks on the pressboard when the needle plate is discharged, calculate the fibre width, porosity, and provide more data results for the partial discharge of the needle-plate and the pressboard degradation study.
2. The development process of white mark is closely related to the development process of partial discharge. There is a certain correspondence between the development stage of partial discharge and the formation stage of white marks. With the increase of pressure time, the area of white marks increases regularly, so that the area of white marks can be used as one of the criteria for the development of discharge of insulated pressboard needle board.
3. Partial discharge has a destructive effect on the fibre diameter, and the fibre diameter decreases with the increase of discharge degree. At the start of the discharge, fibre width was 40.9 μm. Compared with the untreated pressboard, there was little change in fibre diameter. As the degree of partial discharge deepened, the fibres continued to tear and peel under the bombardment of electrons or charged ions. In addition, the "peeling" and "fusing" phenomenon occurred in the fibre, resulting in a significant reduction in the length of the fibre. After breakdown, the fibre diameter dropped to 89.6% of the untreated cardboard.

4. Electrical stress on the insulation pressboard structure presented greater destructive and insulation performance. On the one hand, under the effect of partial discharge, the cellulose hydrogen bond rupture was serious, and the intermolecular forces decreased. On the other hand, as the discharge intensified, the tightness between the fibres decreased, the interlayer pore expansion speed accelerated, and the porosity gradually increased. After breakdown, the porosity reached 1.3 times that of the untreated paperboard.

## REFERENCES CITED

Butcher, M., Neuber, A. A., Cevallos, M. D., Dickens, J. C., and Krompholz, H. (2006). "Conduction and breakdown mechanisms in transformer oil," *IEEE Transactions on Plasma Science* 34(2), 467-475. DOI: 10.1109/tps.2006.872487

Cui, Y., Zhu, L., Ji, S., Cao, P., and Zhang, F. (2017). "Partial discharge development in needle-plane configuration of oil-paper insulation under AC voltage," *IEEE Transactions on Dielectrics and Electrical Insulation* 24(4), 2469-2476. DOI: 10.1109/TDEI.2017.006270

Dong, H., Jiang, Y., Fan, Y. P., Wang, Y., and Gui, G. (2018). "Secondary segmentation extracted algorithm based on image enhancement for intelligent identification systems," *International Journal of Distributed Sensor Networks* 14(12), 155014771881873. DOI: 10.1177/1550147718818737

Du, H., Chen, X., and Xi, J. (2019). "An improved background segmentation algorithm for fringe projection profilometry based on Otsu method," *Optics* 179, 810-818. DOI: 10.1016/j.optcom.2019.06.044

Jia, W. Y., Li, Y. C., and Qu, R. W. (2018). "Automatic food detection in egocentric images using artificial intelligence technology," *Public Health Nutrition* 22(7), 1-12. DOI: 10.1017/S1368980018000538

Khawaja, R., and Blackburn, T. (2009). "Impact of high temperature on partial discharges in oil-impregnated insulation," in: *Australasian Universities Power Engineering Conference*, Adelaide, Australia.

Kolb, J., Joshi, R., Xiao, S. Y. and Schoenbach, K. H. (2008). "Streamers in water and other dielectric liquids," *Journal of Physics D: Applied Physics* 41(23), 234007. DOI: 10.1088/0022-3727/41/23/234007

Li, S. M., Si, W., and Li, Q. Q. (2017). "Partition and recognition of partial discharge development stages in oil-pressboard insulation with needle-plate electrodes under combined AC-DC voltage stress," *IEEE Transactions on Dielectrics and Electrical Insulation* 24(3), 1781-1793. DOI: 10.1109/TDEI.2017.006361

Ma, H., and Guo, J. (2007). "Cut-and-sew algorithm: A new multi-contour reconstruction algorithm," *Journal of Northeastern University* 28(1), 111-114. DOI: 10.3321/j.issn:1005-3026.2007.01.028

Miao, C., Zhang, H., Cheng, J., and Li, T. (2017). "Research on acquisition of leather section images by metallographic sample preparation based on three-dimensional reconstruction," *Journal of the Society of Leather Technologists and Chemists*, 101(4), 195-201.

Mitchinson, P., Lewin, P., and Chen, G. (2008). "A new approach to the study of surface discharge on the oil-pressboard interface," in: *IEEE International Conference on Dielectric Liquids*, Futuroscope-Chasseneuil, France. DOI: 10.1109/ICDL.2008.4622473

Niu, J. L., Shi, Y., Cai, M. L., and Cao Z. X. (2018). "Detection of sputum by interpreting the time-frequency distribution of respiratory sound signal using image processing techniques," *Bioinformatics* 34(5), 820-827. DOI: 10.1093/bioinformatics/btx652

Sun, L., Meng, X. C, Xu, J. C., and Tian Y. (2018). "An image segmentation method using an active contour model based on improved SPF and LIF," *Applied Sciences* 8(12), 2576. DOI: 10.3390/app8122576

Tatsuki, O., Masafumi, Y., and Masayuki, N. (2017). "High voltage insulating material life under partial discharge degradation," in: *2017 IEEE Region 10 Conference*, Penang, Malaysia. DOI: 10.1109/TENCON.2017.8228131

Verma, P., Roy, M., Verma, A., Bhanot, V., and Pandey, O. P. (2004). "Assessment of degradation of transformer insulation paper by SEM and X-RD techniques," in: *Proceedings of the 2004 IEEE International Conference on Solid Dielectrics*, Toulouse, France. DOI: 10.1109/ICSD.2004.1350516

Vincent, L., and Soille, P. (1991). "Watersheds in digital spaces: an efficient algorithm based on immersion simulations," *IEEE Transactions on Pattern Analysis and Machine Intelligence* 13(6), 583-598. DOI: 10.1109/34.87344

Wang, Y. Q., Wang, Y.J, and Jiang, X. L. (2018). "The microscopic morphology of insulation pressboard: an image processing perspective," *Cellulose* 25(5), 1-15. DOI: 10.1007/s10570-018-1768-5

Wang, Y. Q., Luo, Y., Wang, Y.J, and Fei, R.Y. (2019). "Partial discharge damage mechanisms in laminated oil-paper insulation," *Cellulose* 26(9), 1-12. DOI：10.1007/s10570-019-02470-5

Wang, Y. Q., Luo, Y., Guan, J., and Ding, R. J. (2020). "Dielectric properties of epoxy resin impregnated paper insulation in different stages of partial discharge development," *Polymer Composites* 41(1), 360-368. DOI:10.1002/pc.25375

Wang, Y. Q., Zhang, X., and Jiang, X. L. (2019). "Effect of aging on material properties and partial discharge characteristics of insulating pressboard," *BioResources* 14(1), 1303-1316. DOI: 10.15376/biores.14.1.1303-1316

Wei, Y. H., Zhu, M. X., You, X. Y., Deng, J. B., Mu, H. B., and Zhang, G. J. (2015). "Partial discharge characteristics and trap parameters analysis of oil-paper after thermal aging," in: *2015 IEEE 11th International Conference on the Properties and Applications of Dielectric Materials (ICPADM)*, Sydney, Australia. DOI: 10.1109/ICPADM.2015.7295297

Yan, J. M., Liao, R. J., and Yang, L. J. (2012). "Study on microstructure and electrical properties of oil-impregnated paper insulation after exposure to partial discharge," *European Transactions on Electrical Power* 22(6), 0-0. DOI: 10.1002/etep.600

Yi, X., Wang, Z. D., Perrot, F., and Lashbrook, M. (2011). "Surface treeing on pressboard barriers in synthetic and natural ester liquids under AC stress," in: *IEEE International Conference on Dielectric Liquids*, Trondheim. Norway. DOI: 10.1109/ICDL.2011.6015452

Zainuddin, H., Lewin, P. L., and Mitchinson, P. M. (2013). "Partial discharge characteristics of surface tracking on oil-impregnated pressboard under AC voltages," in: *2013 IEEE International Conference on Solid Dielectrics (ICSD)*, Bologna, Italy. DOI: 10.1109/ICSD.2013.6619774

Article submitted: February 10, 2020; Peer review completed: March 23, 2020; Revised version received and accepted: March 28, 2020; Published: March 31, 2020.
DOI: 10.15376/biores.15.2.3585-3603